Pishniak, D., & Razumnyi, S. (2022). Measured and modeled vertical structure of precipitation during mixed-phase event near the West Coast of the Antarctic Peninsula.
Ukrainian Antarctic Journal, *20*(1), 55—66.
https://doi.org/10.33275/1727-7485.1.2022.689

D. Pishniak *, S. Razumnyi
State Institution National Antarctic Scientific Center, Ministry of Education and Science of Ukraine, Kyiv, 01601, Ukraine
*** Corresponding author:** den.meteo.is@gmail.com

Measured and modeled vertical structure of precipitation during mixed-phase event near the West Coast of the Antarctic Peninsula

Abstract. Precipitation structures are easy to detect, however, the mesoscale atmospheric processes which they reflect are challenging to understand in Polar Regions and hard to model numerically. Currently, the spatial distribution of precipitation can be tracked at the resolution of minutes and seconds. For this purpose, the researchers at the Ukrainian Antarctic Akademik Vernadsky station employ several near-ground measurement systems and the Micro Rain Radar for remote vertical measurements. Measurements show stochastic precipitation variability caused by turbulence, precipitation bands related to the atmospheric processes of its formation, phase transition (melting) zones, and wind shears. The time scale of bands in the stratiform precipitation typically varied in the range of 5—15 minutes and corresponded to the 2—15 km spatial scale of atmospheric circulations according to the modeled parameters of the atmosphere. The Polar Weather Research and Forecast (Polar WRF) model was used to reveal the general atmospheric conditions. We also tested and evaluated its ability to reproduce small structures. A simple method based on typical model variables is proposed to identify the precipitation melting layer in the simulation data, similar to that determined by radars. The results were satisfyingly consistent with the position of the 0 °C isotherm in the model and with the radar measurements. In addition, the method highlighted supercooled mixed-phase precipitation. Modeling showed good results for large-scale processes like atmospheric fronts and general air mass features in the case study. However, even at the 1 km resolution the simulation reproduced thin mesoscale precipitation features smoothly, which sometimes looks unrealistic. As for other precipitation peculiarities, like band inclination, melting layer position, and mixed-phase zones, the Polar WRF model demonstrates high consistency with observations. The model can describe the atmospheric conditions except for the investigation of precipitation-initiating mechanisms, which still is a challenge for modeling at a small scale.

Keywords: bright band, melting layer, mixed-phase precipitation, precipitation bands, reflectivity, wind shear

1 Introduction

The fine structure of precipitation reflects mesoscale atmospheric processes, which are still challenging to understand and represent in numerical models (Paul et al., 2021). High-resolution measurement systems reveal peculiarities of a precipitation structure, whereas state-of-the-art models describe general atmospheric conditions of observed structure formation. Together, these approaches bring us closer to a better understanding of the mesoscale processes and define the gaps in the methodology, which may be especially significant in a multifaceted polar region (Bauer et al., 2015).

This study deals with the vertical Micro Rain Radar (MRR) data. It is a new and cost-efficient tool, recently introduced in Antarctica. Like all other weather radars, the MRR needs to specify the relationship

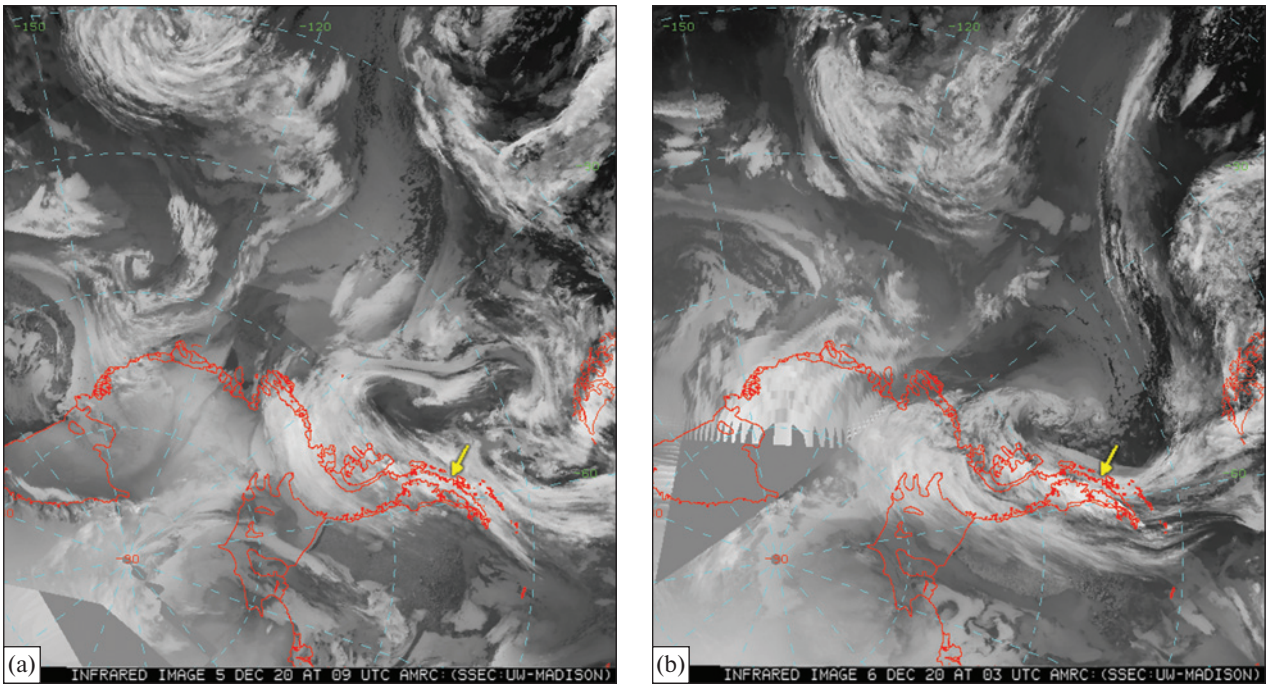

Figure 1. Infrared satellite images of the cloud cover over West Antarctica: (a) — wide cloud band of the warm atmospheric front over the Akademik Vernadsky station (yellow arrow) at 09 UTC on 5 December 2020; (b) — cold front cloud band passing over the Antarctic Peninsula at 03 UTC on 6 December 2020

between reflectivity and precipitation rate (Z-R relationship) to quantify precipitation. Such relationships usually strongly depend on the specific region of the Earth and should be tuned for the typical precipitation of Maritime Antarctica (Souverijns et al., 2017). To describe the precipitation structure, it is enough to take into account the typical Z-R relationship provided by the equipment's software. Durán-Alarcón et al. (2019) have already used the MRR to derive the average precipitation profiles over two locations in Antarctica.

Most precipitation in the polar atmosphere appears in the form of snow. When the temperature of the lower layers of air is positive, the falling snow melts and transforms into rain. The layer where this transformation takes place is called the melting layer (ML) (Drummond et al., 1996), commonly investigated by radars (Brast & Markmann, 2020). Due to the high reflectivity of wet snow, the ML is seen in a radar scan as the well-known "bright band" (BB) (Austin & Bemis, 1950).

The ML height plays a significant role in the Maritime Antarctic region. It determines whether rain or snow will reach the surface and therefore forces ablation or accumulation of glaciers (Lenaerts et al., 2019). Related to the atmospheric processes, precipitation melting also has a secondary influence on the thermal and dynamic state of the local atmosphere through latent heat exchange and cloud microphysics (Szeto et al., 1988; Heymsfield et al., 2015).

Besides the approximately horizontal BB, the radars reveal sporadic vertical bands of precipitation. In a warm atmosphere, they mostly accompany deep convection (convective clouds), where strong turbulence contributes to their formation (Zheng et al., 2019). Although weather radars are comprehensively used in Antarctica (Gorodetskaya et al., 2015), these structures remain without scientific attention.

This work investigates the vertical structure of polar precipitation based on Micro Rain Radar data and Automatic Weather Stations (AWS) measurements, as well as examines the performance of the polar modi-

fication of the Weather Research and Forecast (Polar WRF) model (Hines & Bromwich, 2008) in case of a typical mixed-phase event. The study area belongs to the Maritime Antarctica climate zone near the west coast of the Antarctic Peninsula, and located over the Ukrainian Antarctic Akademik Vernadsky station.

2 Data and methods

2.1 Synoptic situation details

We tested the equipment's ability to detect the ML during rainfall and sensitivity to variable precipitation phases on the data for December 5—6, 2020, with moderate precipitation and a relatively high positive temperature. The key point of the synoptic conditions was a bright warm front passing through the station near the afternoon on December 5 (Fig. 1a), followed by a cold front at 03:00 UTC on December 6 (Fig. 1b). The synoptic situation was close to the classical scheme: a cyclone with a wide, warm sector and a warm conveyor belt along the cold front.

Image source: Antarctic Meteorological Research Center and Automatic Weather Station project, operative information, http://uwamrc.ssec.wisc.edu/data/view-data.php

The meteorological station is located on the small and low (7—10 m a.s.l.) Galindez Island in the Pacific Ocean, 7 km off the west coast of the Antarctic Peninsula. The site has a typical polar marine climate with some traces of the Peninsula barrier effect. As a rule, the open ocean in the summer smooths the air masses' temperature contrast, stabilizing the air surface temperature around the sea surface temperature (−1.0 ... −1.4 °C during the studied days). Therefore, the warm front brought a warming of just 1.5 °C, from −1 to +0.5 °C, and only the warm conveyor belt and turbulence before the cold front reinforced it to +3 °C (Fig. 4).

2.2 In-situ and remote observation sources

Standard 3-hourly weather observations were used to confirm the reliability of automatic systems. Precipitation data were obtained by the Automatic weather station Vaisala AWS-310, including the Vaisala PWD22 combined sensor (1-minute measurement interval),

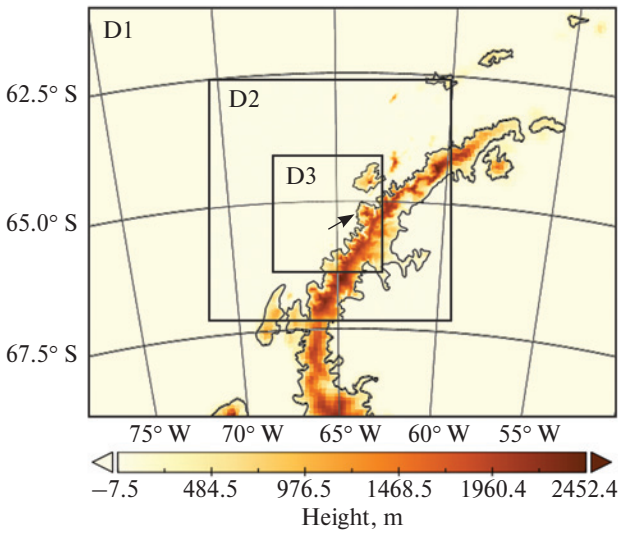

Figure 2. The Polar WRF nested domains and topography. The arrow points at the Akademik Vernadsky station

the Precipitation sensor Lufft WS100 based on the radio reflectivity of precipitation particles (likewise 1-minute interval), and the Micro Rain Radar MRR-PRO. The last one is a K-band (23 GHz) vertically pointing Doppler radar manufactured by METEK. The radar was configured to balance resolution, height, and accuracy: the vertical resolution was 50 m along a scanning depth of 3200 m, with a 30 s measuring interval. Such settings are optimal for polar regions, where precipitation is often weak and appears

Table. Physics parameterization schemes and options for the Polar WRF simulation

Physics	Applied option
Cloud microphysics	Morrison 2-moment
Planetary boundary layer	MYNN2 Nakanishi and Niino
Surface layer	MYNN Nakanishi and Niino
Land surface	Noah Land-surface Model
Cumulus parameterization	Kain-Fritsch (only for D1)
Long wave radiation	RRTMG Fast version
Short wave radiation	RRTMG Fast version
Cloud fraction	On
Heat flux	On
Diffusion	Simple diffusion

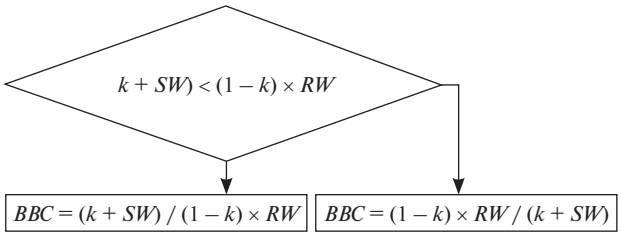

Figure 3. Scheme of the calculation algorithm for the Bright Band definition based on the Polar WRF model data

mostly in the lower layers of the troposphere. For a rain rate estimation by the MRR, we chose the level of 150 m, where the ground influence is negligible.

2.3 Atmospheric model

The case study employed the polar modification of the Weather Research and Forecast model (Polar WRF), version 4.1.1. (Hines & Bromwich, 2008). The simulation was driven by the ECMWF ERA5 reanalysis (0.25°) with 3-hourly data input. The model used nested domains, shaped as described in Pishniak and Beznoshchenko (2020), with a spatial resolution of 9, 3, and 1 km and sizes D1: 130 × 100, D2: 175 × 175, and D3: 232 × 250 grid knots, respectively (Fig. 2). The vertical structure of each domain included 52 levels up to the 15 km height, with 24 levels in the lowest 3 km. Therefore, the vertical resolution of domains changed monotonically from 25 to 350 m at altitudes from Earth surface to 3 km height and remained almost constant above 3 km layer. The time step on each domain was respectively 24, 12, and 6 seconds, assuring computational stability. The physical parameters used after Skamarock et al. (2021) are listed in the Table.

The physical options were the same for all the domains except cumulus parameterization, used only for the first domain (D1). One of the best microphysics parameterizations — the Morrison double-moment scheme for cloud-resolving simulations with ice, snow, rain, and graupel, was applied for a more realistic cloud and precipitation simulation.

To be concise, we show only the results obtained on the third domain (D3), as it has the best resolution. The modeling was started at 12:00 UTC on 4 December, and the first 12 hours were discarded due to the spin-up effect.

2.4 Melting layer determination

There are many approaches to determine the ML-based model data, which are also dependent on certain model capabilities. Thus, Iguchi et al. (2014), in their study of the melting layer performance in the WRF, used sophisticated spectral bin microphysics, generating input to the Radar simulator module of the Goddard Satellite Data Simulator Unit described by Matsui et al. (2009). However, without the necessity of strong correspondence to the radar view, we used a much simpler way to determine the melting layer in a model based on precipitation phase reproduction. To obtain a picture similar to the BB based on the model data, we combined a logical and a mathematical approach to calculate the bright band coefficient (*BBC*). It includes the relationship between the mass content of rain (*RW*) and snow water (*SW*) and the logical reverse of the relationship when it exceeded 1. That highlights volumes in the modeled atmosphere with wet snow (Fig. 3).

Here k is a wet coefficient. We used $k = 0.15$ to assume that the strongest BB appears when precipitation contains 15% liquid and 85% solid water. It follows from the algorithm that the *BBC* assumes values from 0 to 1, where values near 1 means the strongest BB effect and conditions of the ML position.

3 Results

3.1 Model conformity check and observation analysis

First, a conformity check of the simulation was done on the temperature and wind speed in-situ data obtained at the Akademik Vernadsky station (Fig. 4). It showed a distinct correspondence to large-scale synoptic dynamics. The warm air mass following the cyclone's warm front (09—24 UTC on December 5) was the most difficult period for the model, although the temperature deviation was less than 1.5 °C, and the wind speed deviation reached 7 m/s. The model ignored two gust waves near 21 UTC. Such challenges occur when an air mass goes along the rugged Antarctic Peninsula (AP) coast, as is typical for the warm advection at this location. The cold frontal zone,

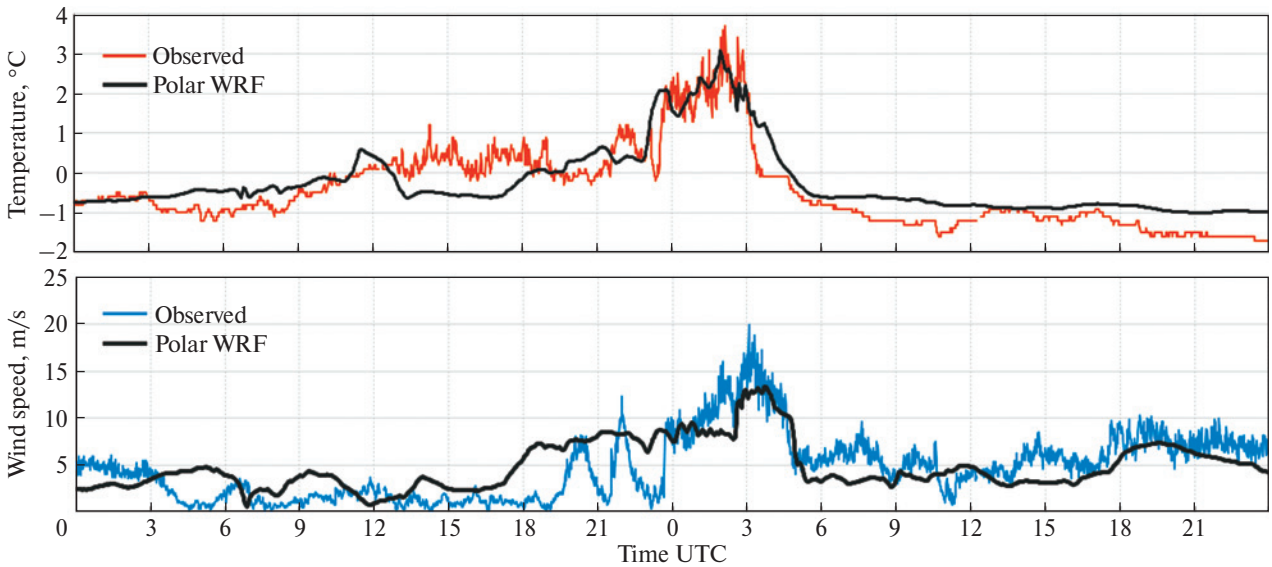

Figure 4. Simulation conformity check on the temperature and wind speed measurements at the Akademik Vernadsky station during the two days of the case study period of December 5—6, 2020

including a warm prefrontal intrusion (warm conveyor belt) and the cold front passing, were simulated almost perfectly (00—06 UTC December 6), and so was the further postfrontal cold air mass. These atmospheric processes came from the open ocean, making them easier to reproduce.

Near-surface high-resolution observations are highly influenced by noise from the occasional turbulence mixing, and this also applies to high-resolution precipitation measurements by Lufft WS100 and Vaisala PWD22. As the precipitation formation processes often occur at small scales, separating them after the boundary layer turbulence distortion is challenging. Therefore, the instrument like the MRR is needed to reveal processes at the height of precipitation formation. The MRR allows to see the vertical structure of the precipitation in time and height, defining a spatial scale of the atmospheric perturbations when the wind speed is known.

A wide frontal zone of the warm atmospheric front had already started precipitating by the beginning of December 5. At 08 UTC, the MRR detected a melting zone in the snowfall precipitation at a 500 m; at 10 UTC, other sensors also detected the wet snow; at 12 UTC, observers noted snow with rain, and at 15 UTC, light rain and drizzle in keeping with the warm sector of the cyclone (Fig. 5a). Near 00 UTC on 6 December, precipitation of the cold frontal zone began. A warm conveyor belt was detected by temperature rising to 3 °C and the highest melting zone position, which rose above 1 km according to the MRR measurements. During the next 3 hours, the ML layer went down to the surface, which meant that cold advection started in the depth of the atmosphere. Finally, at 03 UTC on December 6, the surface air temperature dropped sharply (Fig. 4), denoting the passing of the cold front itself. The rest of the time was associated with a cold air mass and oceanic convective precipitation.

Precipitation estimation in Polar Regions is always challenging due to the strong winds and diversity of snowflake shapes. Therefore, all three available sensors often differ strongly. The WS100 and the MRR (150 m) operate on the radiolocation principle and usually have very similar results. The MRR showed an unrealistically strong precipitation rate only when the melting snow occurred. The Vaisala PWD22 sensor overestimated precipitation related to both radar sensors, especially during dry snow periods. On the other hand, the modeled precipitation rate at the grid point nearest to the Akademik Vernadsky station had

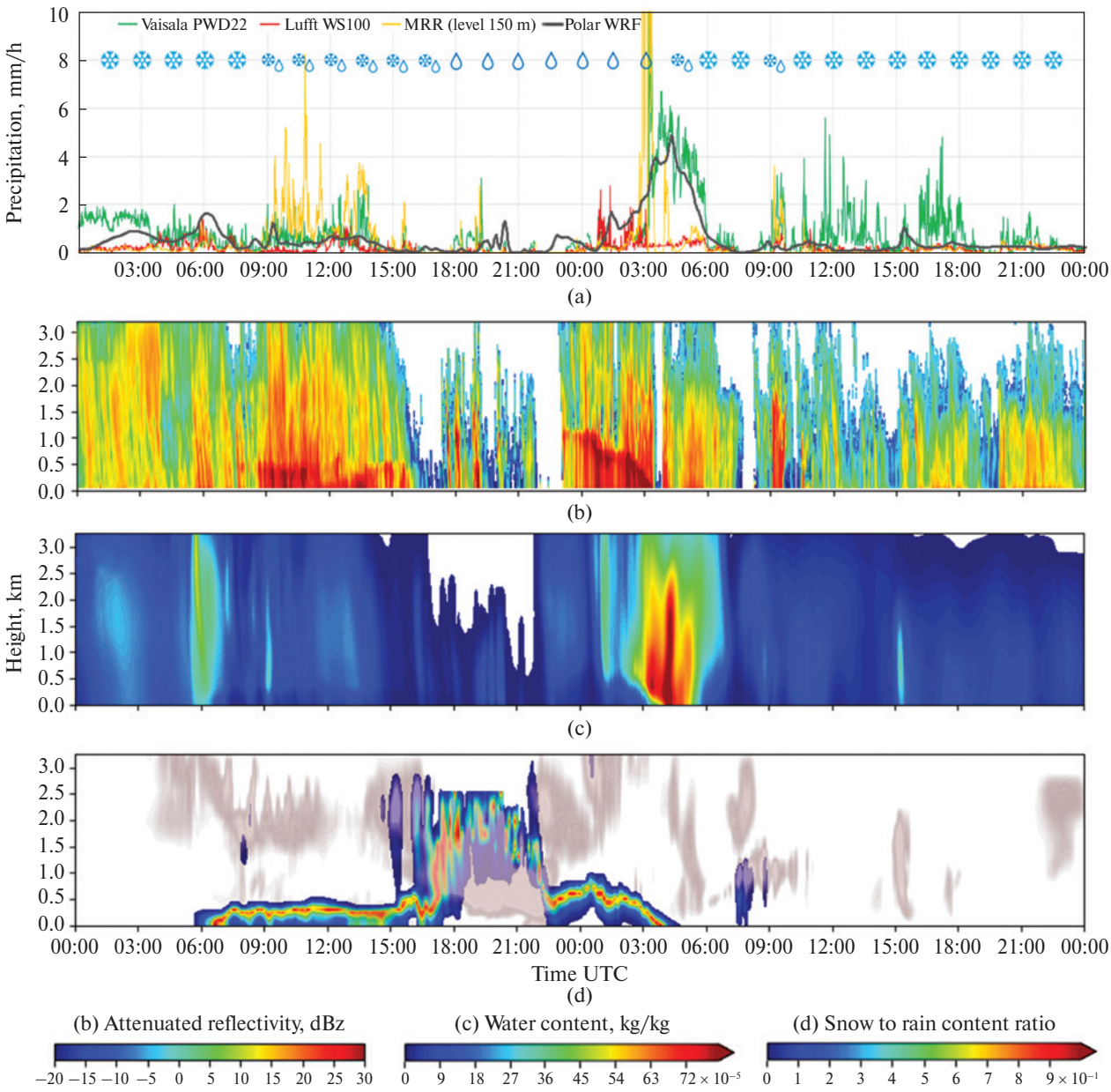

Figure 5. Timeline of the precipitation characteristics during 5—6 December 2020: (a) near-surface measured and modeled values of precipitation rates and the observed phase; (b) MRR time-vertical cross-section of the attenuated reflectivity; (c) precipitable water content (mixing ratio) in the atmosphere including rain, snow, and graupel, derived from Polar WRF; (d) snow-to-rain ratio indicating the "bright band" or melting layer position, calculated based on the Polar WRF data. Gray filling denotes the cloud water content corresponding to dense clouds

a similar curve to the measurements in general (Fig. 5a). For some periods, its curve closely followed the data of the radiolocation sensors, but at the cold front precipitation (00—06 UTC December 6), the modeled precipitation became more similar to the PWD22 combined sensor.

The measured vertical structure of precipitation is shown in Figure 5b. The maximums mostly relate to

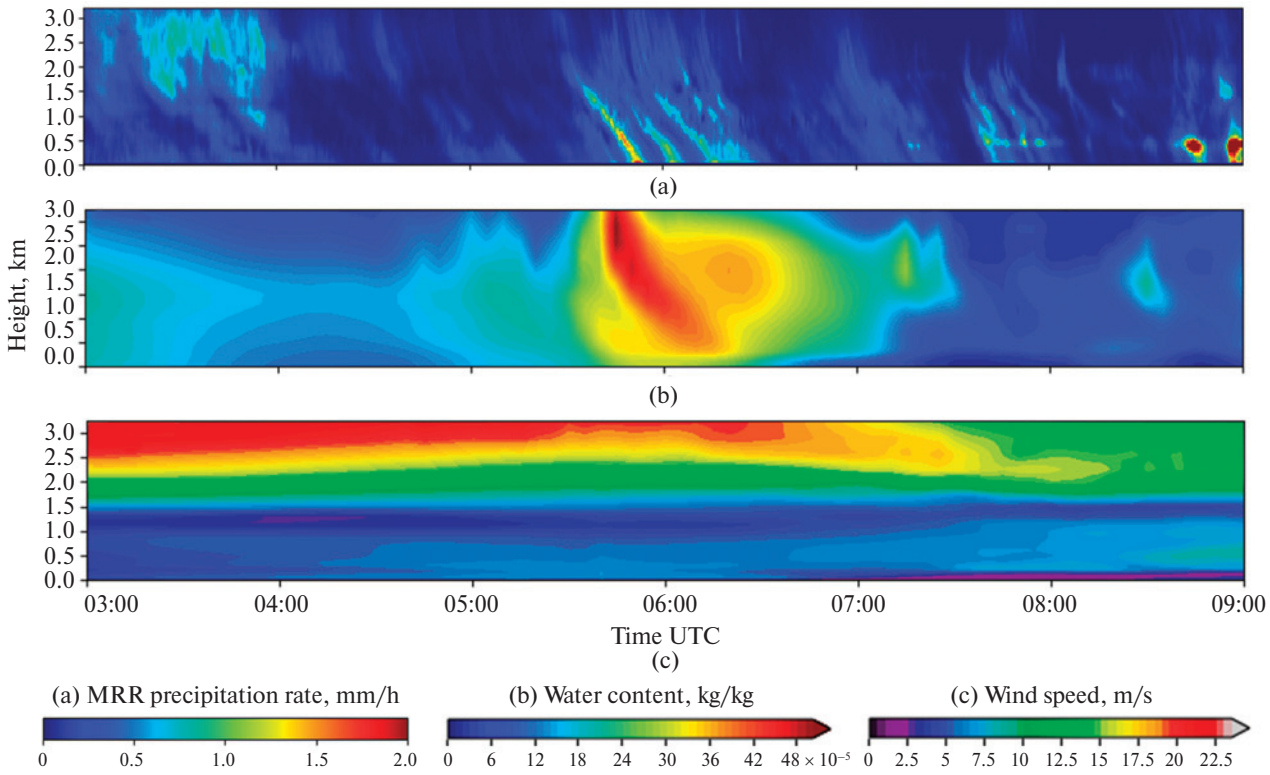

Figure 6. A subcase of precipitation band inclination. (a) MRR rain rate, calculated from measured reflectivity (built-in option); (b) precipitable water content derived from the Polar WRF, the same as in Figure 5c; (c) the wind speed modeled in Polar WRF demonstrates strong shear at 2 km height

BB. There are many methods for automatic detection of the ML, but they can be found easily on the radar reflectivity diagrams by the BB position (Brast & Markmann, 2020). The current case occurred from 08 UTC December 5 to 03 UTC December 6, when wet snow and rain were observed. The other peculiarity is that even the stratiform precipitation of a warm front had a stripe structure stretched from more than 2—3 km at the height of its formation to the ground level. A similar pattern persisted for the cold air mass only with a lower height of precipitation initiation. This result confirms that the high-frequency variability of massive precipitation is caused by processes of the free atmosphere and the boundary layer turbulence.

Atmospheric modeling with 1 km resolution was applied to reproduce vertical bands in the field of precipitable water content (Fig. 5c). Occasionally, the results look more successful, for example, for the warm air mass with weak bands (18—21 UTC 5 December) and the cold front structure, but at other times the field of precipitable water was unrealistically smoothed. Over the beginning of the period of precipitation, the bands are significantly inclined. Therefore, we examine this event as a subcase below.

3.2 Precipitation bands' inclination

The period from 03 to 09 UTC on December 5, was chosen for a more detailed investigation of precipitation bands' inclination, found in the MRR diagrams. The variable of the rain rate from the MRR scope (Fig. 6a) was selected as the most similar to the WRF precipitable water content shown in Figure 6b. The model attempts to reproduce the precipitation bands, and it is most successful near the 05—06 UTC, but in any case, it looks wider and much smoother than in reality. Nevertheless, the modeled bands have a very similar inclination angle, and thus descent trajectories of precipitation. This result confirms the correct

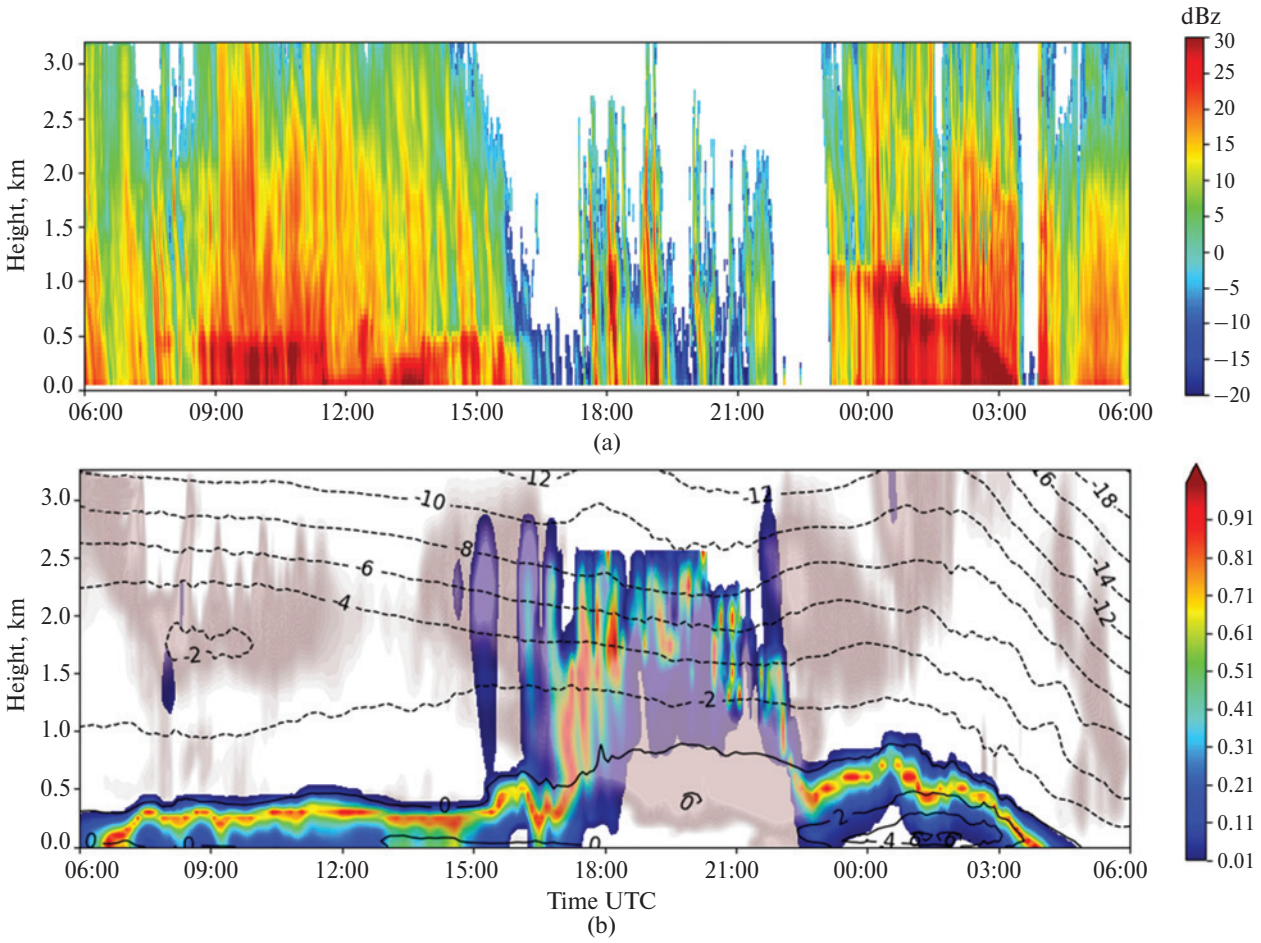

Figure 7. Subcase of mixed-phase precipitation and melting layer time on 5—6 December 2020. (a) MRR attenuated reflectivity; (b) snow-to-rain ratio, the same as Figure 5d but with isotherms of temperature in °C. Gray shaded areas denote the presence of cloud water content

reproduction of precipitation particles, their phase, size, and descent speed in the model.

The noticeable change of the inclination angle at 1.5 km (Fig. 6a, b) indirectly indicates strong wind shear that should exist near this altitude. The Polar WRF simulation has already confirmed the wind shear in the 1.5—2 km layer on a scalar wind speed diagram (Fig. 6c). In this layer, the wind rapidly increased from 6 to 13 m/s.

3.3 The melting layer

A general picture of the ML is seen in Figure 5b, d. To simplify the analysis, the period from 06 UTC December 5 to 06 UTC December 6 was zoomed-in in Figure 7. The radar recorded the appearance of the BB and the corresponding ML near 07:40 UTC at 0.4—0.5 km height. It was seen throughout the warm front precipitation period but not very stable. Some uncertainties were found because the vertical temperature gradient was not strong enough, and precipitation still reached the ground as wet snow. The ML behavior is unknown during the 16—23 UTC period of the warm air mass, as light precipitation seemed to have appeared from supercooled liquid water at high levels, directly in the form of drizzle. The ML definitely re-appeared at the 1 km height when the cold front precipitation arrived. Over the next 4 hours,

the ML quickly went down. It reached the ground at 03 UTC on December 6, and the near-surface rain was converted to snow.

The proposed approach for ML detection in the model data highlights it simultaneously as it is observed on the radar (Fig. 7b), with the only remark that the maximum bright level tends to slightly underestimate the height, which is a subject for discussion. In the warm air mass period from 17 to 22 UTC, the algorithm showed supercooled water (probable drizzle) at 2 km height rather than the ML. This is indicated by the vertical temperature distribution. As can be seen in Figure 7b, normally, the ML closely follows the 0 °C isotherm. The comparison of radar and model data shows that supercooled water mixed with ice crystals can also create strong reflectivity spots but appear more randomly deep in the atmosphere.

The model simulated an interesting event of a warm conveyor belt between 00 and 03 UTC. A narrow low-level jet was created with a temperature maximum near 6 °C explaining why the ML rose then. About this time, the MRR showed a higher position of the BB than the model, which can mean a thicker warm low-level jet compared to the model.

4 Discussion

A typical period of precipitation bands derived from the MRR measurements is 5—15 minutes (Fig. 6a). This is equal to the 5—15 km spatial scale of the atmospheric processes developed at approximately 2.5 km, where the wind speed is 15—20 m/s (Fig. 6c). In the lower layer (below 1.5 km), where the wind speed is near 5 m/s, the process scale is 2—5 km, but the measurements show that precipitation initializes mainly from the middle layer of the troposphere. In any case, this spatial scale is in the resolving range of the numerical model, but the model mostly ignores the bands in stratiform clouds or tries to represent them very smoothly (Fig. 6b). Hence, the modeling resolution should be increased. Although, Chyhareva et al. (2021) showed that the Polar WRF model has good applicability in the simulation of the precipitation phase transitions for this region.

The proposed ML detection algorithm based on the model's ratio of liquid to solid precipitation with the coefficient of 0.15 (equal to 1/5 proportion) showed good results with only a small underestimation of height. The coefficient can correct the height, but a further decrease can bring a loss of reliability. The obtained Bright Band follows the 0 °C isotherm most of the time, except for 17—22 UTC (Fig. 7b), when regions of supercooled water appear at a higher level. Hines et al. (2021) reported difficulties in WRF cloud microphysics parameterizations representing the supercooled water at temperatures below −20 °C. In the discussed subcase, the supercooled water may definitely be present in the model. If this result is undesirable, a condition operator for the temperature can be added to the algorithm. In our case, the BB position tends to be 150—300 m below the 0 °C isotherm, but Thurai et al. (2003) and Awaka et al. (2009) obtained its position 300—500 m below the 0 °C isotherm. Their results can be explained by lower-resolution models and tropical regions of investigation, where the isotherm is in the thin air layer above 2 km.

The uncertainty with precipitation measurements still exists in polar regions, and modeling cannot help to solve this problem. The authors agree that using data collected from only one site over a short period of the case study is not enough for strong conclusions about the model's performance in the whole range of atmospheric conditions.

5 Conclusions

The Polar WRF model, including high-quality microphysics parameterizations, reproduces quite well the BB and ML positions and, consequently, the melting process in the case of polar stratiform precipitation. It is confidently confirmed by the MRR data. Furthermore, the model result partly reproduces the formation of supercooled liquid precipitation in the warm air mass of the cyclone. However, this process is weakly confirmed by the MRR measurements because of the higher recognition uncertainty.

High-frequency variability of precipitation intensity, detected in near-surface measurements, is caused

by the boundary layer turbulence as well as the variability of the precipitation formation in a free atmosphere. The temporal scale of these processes typically varied in the range of 5—15 minutes, corresponding to a 2—15 km spatial scale of atmospheric circulations. Such processes are presented almost every time in massive precipitation and produce quasi-vertical reflectivity bands on the MRR diagrams. The WRF model simulation with 1 km resolution can reproduce these mesoscale precipitation features very smoothly and with low confidence. Hence, experiments with a higher model resolution are desirable for investigating vertical band formation in stratiform precipitation. On the other hand, the model shows similar bands' inclination, which indirectly confirms the appropriate wind shear and the fall speed of the precipitation particles.

The modeled atmosphere parameters such as temperature, wind, and humidity may considerably improve our understanding of the observed precipitation features in complicated weather cases.

Author contributions. DP: main idea, editing, post-processing of model output, writing the article. SR: processing of in-situ and remote sensing measurements.

Acknowledgments. The work was carried out within the framework of the State Special-Purpose Research Program in Antarctica for 2011—2023. The authors thank Anastasia Chyhareva for her technical support in obtaining research data.

Conflict of Interest. The authors declare that they have no conflict of interest.

References

Austin, P. M., & Bemis, A. C. (1950). A quantitative study of the "bright band" in radar precipitation echoes. *Journal of the Atmospheric Sciences*, *7*(2), 145—151. https://doi.org/10.1175/1520-0469(1950) 007<0145:AQSOTB>2.0.CO;2

Awaka, J., Iguchi, T., & Okamoto, K. (2009). TRMM PR standard algorithm 2A23 and its performance on bright band detection. *Journal of the Meteorological Society of Japan. Ser. II*, *87A*, 31—52. https://doi.org/10.2151/jmsj.87A.31

Bauer, H-S., Schwitalla, T., Wulfmeyer, V., Bakhshaii, A., Ehret, U., Neuper, M., & Caumont, O. (2015). Quantitative precipitation estimation based on high-resolution numerical weather prediction and data assimilation with WRF — a performance test. *Tellus A: Dynamic Meteorology and Oceanography*, *67*(1), 25047. https://doi.org/10.3402/tellusa.v67.25047

Brast, M., & Markmann, P. (2020). Detecting the melting layer with a micro rain radar using a neural network approach. *Atmospheric Measurement Techniques*, *13*(12), 6645—6656. https://doi.org/10.5194/amt-13-6645-2020

Chyhareva, A., Gorodetskaya, I., Krakovska, S., Pishniak, D., & Rowe, P. (2021). Precipitation phase transition in austral summer over the Antarctic Peninsula. *Ukrainian Antarctic Journal*, 1, 32—46. https:// doi.org/10.33275/1727-7485.1.2021.664

Drummond, F. J., Rogers, R. R., Cohn, S. A., Ecklund, W. L., Carter, D. A., & Wilson, J. S. (1996). A new look at the melting layer. *Journal of the Atmospheric Sciences*, *53*(5), 759—769. https://doi.org/10.1175/1520-0469(1996)053<0759:ANLATM>2.0.CO;2

Durán-Alarcón, C., Boudevillain, B., Genthon, C., Grazioli, J., Souverijns, N., van Lipzig, N. P. M., Gorodetskaya, I. V., & Berne, A. (2019). The vertical structure of precipitation at two stations in East Antarctica derived from micro rain radars. *The Cryosphere*, *13*, 247—264. https://doi.org/10.5194/tc-13-247-2019

Gorodetskaya, I. V., Kneifel, S., Maahn, M., van Tricht, K., Thiery, W., Schween, J. H., Mangold, A., Crewell, S., & van Lipzig, N. P. M. (2015). Cloud and precipitation properties from ground-based remote-sensing instruments in East Antarctica. *The Cryosphere*, *9*, 285—304. https://doi.org/10.5194/tc-9-285-2015

Heymsfield, A. J., Bansemer, A., Poellot, M. R., & Wood, N. (2015). Observations of ice microphysics through the melting layer. *Journal of the Atmospheric Sciences*, *72*(8), 2902—2928. https://doi.org/10.1175/JAS-D-14-0363.1

Hines, K. M., & Bromwich, D. H. (2008). Development and testing of polar Weather Research and Forecasting (WRF) Model. Part I: Greenland ice sheet meteorology. *Monthly Weather Review*, *136*(6), 1971—1989. https://doi.org/10.1175/2007MWR2112.1

Hines, K. M., Bromwich, D. H., Silber, I., Russell, L. M., & Bai, L. (2021). Predicting frigid mixed-phase clouds for pristine coastal Antarctica. *Journal of Geophysical Research: Atmospheres*, *126*(23), e2021JD0 3 5112. https://doi.org/10.1029/2021JD035112

Iguchi, T., Matsui, T., Tao, W.-K., Khain, A. P., Phillips, V. T. J., Kidd, C., L'Ecuyer, T., Braun, S. A., & Hou, A. (2014). WRF–SBM simulations of melting-layer structure in mixed-phase precipitation events observed during LPVEx. *Journal of Applied Meteorology and Climatology*, *53*(12), 2710—2731. https://doi.org/10.1175/JAMC-D-13-0334.1

Lenaerts, J. T. M., Medley, B., van den Broeke, M. R., & Wouters, B. (2019). Observing and modeling ice sheet sur-

face mass balance. *Reviews of Geophysics*, *57*(2), 376—420. https://doi.org/10.1029/2018RG000622

Matsui, T., Zeng, X., Tao, W.-K., Masunaga, H., Olson, W. S., & Lang, S. (2009). Evaluation of long-term cloud-resolving model simulations using satellite radiance observations and multifrequency satellite simulators. *Journal of Atmospheric and Oceanic Technology*, *26*(7), 1261—1274. https://doi.org/10.1175/2008JTECHA1168.1

Paul, S., Wang, C. C., Tseng, L. S., Lee, D. I., Hong, J. S., Leou, T. M. (2021). Evaluation of rainfall forecasts by three mesoscale models during the Mei-yu season of 2008 in Taiwan. Part I: Subjective comparison. *Asia-Pacific Journal of Atmospheric Sciences, 57*(4), 817—838. https://doi.org/10.1007/s13143-021- 00229-2

Pishniak, D., & Beznoshchenko, B. (2020). Improving the detailing of atmospheric processes modelling using the Polar WRF model: a case study of a heavy rainfall event at the Akademik Vernadsky station. *Ukrainian Antarctic Journal*, 2, 26—41. https://doi.org/10.33275/1727-7485.2.2020.650

Skamarock, W. C., Klemp, J. B., Dudhia, J., Gill, D. O., Liu, Z., Berner, J., Wang, W., Powers, J. G., Duda, M. G., Barker, D., & Huang, X.-Y. (2021). A description of the advanced research WRF Model Version 4.3 (No. NCAR/TN-556+STR). https://doi.org/10.5065/1dfh-6p97

Souverijns, N., Gossart, A., Lhermitte, S., Gorodetskaya, I. V., Kneifel, S., Maahn, M., Bliven, F. L., & van Lipzig, N. P. M. (2017). Estimating radar reflectivity — snowfall rate relationships and their uncertainties over Antarctica by combining disdrometer and radar observations. *Atmospheric Research*, *196*, 211—223. https://doi.org/10.1016/j.atmosres.2017.06.001

Szeto, K. K., Lin, C. A., & Stewart, R. E. (1988). Mesoscale circulations forced by melting snow. Part I: Basic simulations and dynamics. *Journal of the Atmospheric Sciences*, *45*(11), 1629—1641. https://doi.org/10.1175/1520-0469(1988)045<1629:MCFBMS>2.0.CO;2

Thurai, M., Deguchi, E., Iguchi, T., & Okamoto, K. (2003). Freezing height distribution in the tropics. *International Journal of Satellite Communications and Networking*, *21*(6), 533—545. https://doi.org/10.1002/sat.768

Zheng, J., Zhang, P., Liu, L., Liu, Y., & Che, Y. (2019). A study of vertical structures and microphysical characteristics of different convective cloud—precipitation types using Ka-band millimeter wave radar measurements. *Remote Sensing*, *11*(15), 1810. https://doi.org/10.3390/rs11151810

Received: 18 April 2022
Accepted: 5 July 2022

Д. Пішняк*, С. Разумний

Державна установа Національний антарктичний науковий центр,
Міністерство освіти і науки України, м. Київ, 01601, Україна

*** Автор для кореспонденції:** den.meteo.is@gmail.com

Виміряна та змодельована вертикальна структура опадів під час випадку опадів змішаної фази поблизу західного узбережжя Антарктичного півострова

Реферат. Структури опадів, які зазвичай легко ідентифікуються, відображають собою мезомасштабні процеси в атмосфері. У полярних регіонах ці процеси є проблемними для розуміння та відтворення у чисельних моделях. Нові автоматичні вимірювальні технології можуть забезпечувати моніторинг опадів у просторі та часі з інтервалом дискретності у хвилини чи навіть секунди. Так, і на Українській антарктичній станції «Академік Вернадський» працює кілька наземних вимірювальних систем та Micro Rain радар, призначений для дистанційного вимірювання вертикального розподілу опадів. Дані цих приладів показують стохастичну мінливість інтенсивності опадів, зумовлену турбулентністю, смуги опадів відповідно до процесів їх формування, а також зони зміни фази (танення) та вертикальні зсуви вітру. Часовий масштаб смуг у облогових опадах зазвичай варіював у межах 5—15 хвилин, що відповідало просторовому масштабу процесів 2—15 км (відповідно до отриманих параметрів змодельованої атмосфери). Модель Polar Weather Research and Forecast (Polar WRF) була використана для отримання загальних умов у атмосфері та для перевірки здатності самої моделі у відтворенні дрібномасштабних процесів. Для виділення шару танення снігу в даних моделювання, аналогічного тому, який ідентифікують радіолокатори, був запропонований простий спосіб на основі базових змінних моделі. Спосіб продемонстрував добру узгодженість результату як щодо положення 0 °C ізотерми в моделі, так і загалом з діаграмою радіолокаційних вимірів. Крім того, також виділяється наявність переохолоджених опадів змішаної фази. Модель дозволила отримати узгоджений результат для процесів

великого масштабу, таких як атмосферні фронти та загальні особливості повітряних мас у цьому випадку дослідження. Але навіть роздільна здатність симуляції в 1 км відтворила дрібні мезомасштабні особливості структури опадів дуже згладжено, що виглядає далеким від реальності. Щодо інших особливостей опадів, таких як нахил смуг опадів, положення шару танення і зон змішаної фази, модель Polar WRF демонструє відносно високу відповідність натурним вимірюванням. Це загалом підтверджує, що модель може використовуватись для опису атмосферних умов, окрім механізмів ініціації опадів, які залишаються проблемою для моделювання на такому масштабі і просторовій роздільній здатності.

Ключові слова: відбивна здатність, зсув вітру, опади, опади змішаної фази, смуги опадів, шар танення, яскрава смуга опадів